Diffusion Transport in Reconstructed Semi-Crystalline Structure of Polyolefins

*Hana Hajová, Richard Pokorný, Juraj Kosek**

Summary: Diffusion of penetrants (e.g., monomers) in polyolefins is important not only in their manufacturing and down-stream processing, but also in packaging and separation applications. We propose a general methodology linking the semi-crystalline structure of polyolefins to their application properties. This methodology comprises of AFM imaging of semi-crystalline structure, reconstruction of 3D replica of semi-crystalline polymer and calculation of application properties (e.g., diffusivity) depending on 3D morphology. Our algorithm is capable to achieve realistic crystallinities of reconstructed samples up to 70% and to reconstruct spherulites with preferential orientation of lamellae. We demonstrate and discuss difficulties experienced during AFM imaging of HDPE morphology, particularly the dependence of resulting AFM image representing the distribution of crystalline domains on the sample preparation including etching.

Keywords: oxygen plasma etching; polyolefins; reconstructed spherulite; semi-crystalline morphology

Introduction

Most of the commercially produced polyolefins like HDPE, LDPE, LLDPE and PP have semi-crystalline structure. Crystalline phase is present in the form of primary domains of characteristic thickness approx. 10 nm, such as lamellae or fringed micelles. These primary crystalline domains are separated by amorphous polymer. The lateral growth of crystalline domains creates spherulites or other secondary structures of characteristic size in the range of 0.1 to 10 μm. Semi-crystalline structure of polyolefins is predetermined by the molecular architecture of polymers, e.g., by distributions of branching and copolymer content, and by conditions applied to sample during its crystallization. Semi-crystalline structure of polyolefins predetermines their mechanical, optical and penetrant-diffusion properties. Diffusion of penetrants (e.g., monomers) in polyolefins is important not only in their manufacturing and down-stream processing, but also in packaging and separation applications.

Morphology of semi-crystalline samples can be characterized either by direct visualization methods (electron microscopy, AFM, imaging in cross-polarized light) or by integral characteristics (DSC, X-ray scattering, Raman spectroscopy), cf. Slusarczyk,[1] Zhou and Wilkes.[2] The outcomes of morphology characterization strongly depend on the process of sample preparation.[3] In this paper we present morphology analysis of either nascent polyolefin powder collected at the reactor outlet or of common compact specimens. We demonstrate how the boundaries of spherulites can be mapped by AFM and how the type of etching procedure affects the observed distribution of crystalline domains. The goal of AFM characterization of semi-crystalline morphology is to obtain suitable morphology descriptors capable to describe size distribution and arrangement of crystalline domains.

Department of Chemical Engineering, Institute of Chemical Technology Prague, Technická 5, 166 28 Prague 6, Czech Republic
Fax: +420 22044 4320; E-mail: Juraj.Kosek@vscht.cz

The objective of the modeling part is to reconstruct the artificial spatially 3D spherulites. The reconstructed spherulites shall be statistically equivalent to experimental samples, i.e., they should posses the same morphology descriptors as real samples. Reconstructed spherulites or other types of semi-crystalline structures allow us to calculate effective diffusivity of penetrant in semi-crystalline polymer and this effective diffusivity could be compared to experimental measurements in order to independently validate reconstructed 3D semi-crystalline structure. In the simulation of reconstruction we extended the work of Mattozzi et al.,[4,5] who were capable to reconstructed spherulites with a crystallinity up to 30%. In our approach we can achieve realistic crystallinities up to 70%. Moreover, our advanced reconstruction algorithm allows to reconstruct spherulites with preferential orientation of lamellae, thus supporting anisotropic penetrant-in-polymer diffusion.

In this paper we report on the current progress in reconstruction of semi-crystalline media as well as some critical points that require further effort. The work has not been finished yet because the quantitative comparison of the morphology of semi-crystalline polyolefins with the reconstructed spherulite hasn't been made yet due to difficulties in evaluation morphology descriptors from AFM images of etched polymer samples. Nevertheless, the proposed methodology has a good potential as it shall allow to predict structure property relationships not only for penetrant diffusion, but also for mechanical and optical properties of polyolefins.

Polyolefin Morphology Investigated by AFM

The morphology of semi-crystalline polyolefins can be characterized by several methods including DSC, X-ray scattering and electron microscopy measurements. The method employed in our investigation is Atomic Force Microscopy (AFM). AFM allows for simultaneous imaging of the topology and of the distribution of hard (i.e., crystalline) and soft (i.e., amorphous) phases on the sample surface.[6] This imaging can be conducted with nanometer resolution. The capabilities of AFM are much broader than described here – AFM also allows to characterize distribution of local adhesive, friction and elastic properties.

In order to obtain high-quality AFM images of semi-crystalline polymers, we need to prepare perfect quality planar cut through the sample. Planar cut was made at cryo conditions on microtome Leica UC6 with AFM-grade diamond knife from DIATOME company. After microtomy the sample surface gets somewhat rough (± 50 nm) due to uneven thermal expansion of amorphous and crystalline phases. AFM phase image of microtomed HDPE sample A ($\rho = 0.941\ \mathrm{g\,cm^{-3}}$) scanned at room temperature is displayed in Figure 1. We can distinguish boundaries of well-separated polyhedral zones that likely represent cross-sections of individual spherulites – dark regions between polyhedral zones are softer. The polyhedral zones have a diameter of 0.1 to 0.5 μm. Standard imaging of spherulites in cross-polarized light is limited to thin films crystallized at well-controlled artificial conditions and is applicable only to

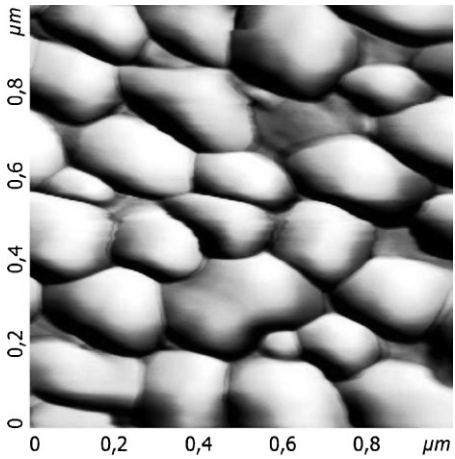

Figure 1.
AFM phase image of HDPE sample A with well visible boundaries of polyhedral zones. Polyhedral zones likely represent individual spherulites.

spherulites larger than several microns.[7] Thus imaging of spherulite sizes, that strongly affects optical properties of polyolefins, can be conveniently performed by AFM.

Primary crystallites are not visible in Figure 1 even at large magnification. In order to uncover the semi-crystalline domains one has to conduct etching of sample surface to selectively remove the surface layer of amorphous polymer. Etching procedures are only partially selective as they remove amorphous phase faster than the crystalline one. Moreover, the etching of crystallites depends on their spatial orientation with respect to sample surface. Images of semi-crystalline morphology thus depend not only on sample properties, but also on AFM parameters of scanning and on etching time, i.e., on the thickness of the layer of amorphous phase being removed prior to AFM measurements.

Wet permanganic etching is the classical method performed with the typical etching solutions composition of 4 wt. % H_2O, 26 wt. % H_3PO_4, 69 wt. % H_2SO_4 and 1 wt. % $KMnO_4$. The spherulite banding pattern is clearly seen in AFM images (Figure 2) of wet-etched surfaces. The images show the regular twisting of lamellar ribbons that produce the banding pattern. Bright rings in the height image (elevated regions) consist of lamellae lying flat, whereas dark rings are composed of lamellae standing on the edge. AFM imaging of wet-etched samples is a widely used method[8] because it provides us with the information about long-distance ordering of primary crystallites. However, this method is not suitable for obtaining of images required in automatic evaluation of morphological descriptors due to poor contrast.[7] AFM images of wet-etched samples published in the literature have a quality comparable to our images. Roughness of wet-etched samples in Figure 2 is ± 100 nm.

Let us remind that our immediate goal is the development of the methodology capable of evaluation of morphology descriptors and not the visual analysis of semi-crystalline polymers from AFM images. Since the outcome of wet-etching is not suitable for systematic analysis of samples by morphology descriptors, we employed an alternative etching method in oxygen plasma.

Perfectly planar surfaces of PE samples were etched by oxygen plasma in the apparatus PlasmaPrep II for various periods of time. Etching has semi-selectively removed the amorphous polymer layer and exposed thus the crystalline phase as

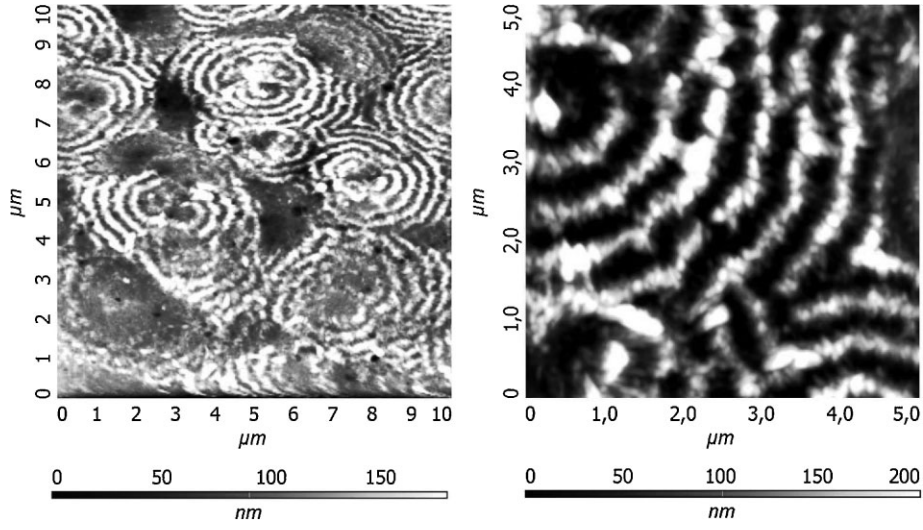

Figure 2.
AFM topology images of the spherulite banding pattern, Sample B (HDPE, $\rho = 0.9394\ g\ cm^{-3}$).

shown in Figure 3. Phase images show the morphology of various twisting, branching and stacking lamellar ribbons, the small dark regions contain the residual amorphous phase. Typical crystallinity of PE is 60 to 70 vol.%, therefore the content of amorphous (dark) phase in Figure 3 is small. Quantity of the residual amorphous phase also depends on etching time. Moreover, the finite diameter of AFM tip distorts the image as it broadens the thickness of crystalline lamellae. The preferential orientation of lamellae ribbons in PE film sample is shown in Figure 4.

Finally Figure 5 shows the granular-like morphology of HDPE sample. We can observe brighter regions of crystal phase separated by the amorphous phase. The morphology shown in Figure 5 is not the ''fringed micelle'' morphology because the characteristic size of crystalline domains is 20 to 70 nm, thus it is much larger than in the ''fringed micelle'' concept.

The individual primary crystalline domains can be visually clearly recognized in Figure 3-5 in difference from wet-etched samples. Figure 3-5 indicate that there are several types of morphologies of semi-crystalline polymers present in the same HDPE polymer. Microtomy of sample B visualized in Figure 3-5 was conducted under different angles. Moreover, Figure 3-5 display polymer sample subjected to different periods of plasma etching and scanned by AFM at various locations of the sample. These Figures nicely illustrate the difficulty and ambiguity of morphology characterization.

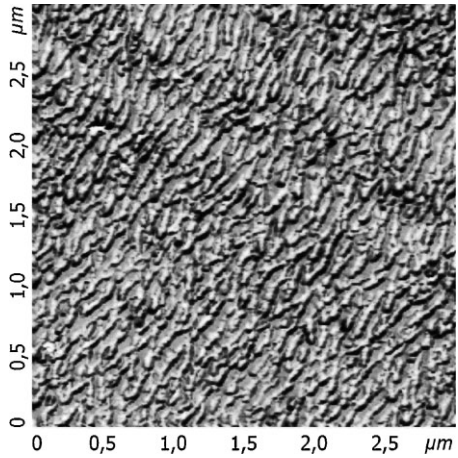

Figure 4.
AFM phase image of HDPE sample B ($\rho = 0.9394\ g\ cm^{-3}$) of the lamellar ribbons in preferential orientation.

Reconstruction of Crystalline-Phase Morphology of Semi-Crystalline Polymers

Purely geometrical approach to reconstruction of a single spherulite consisting from lamellae was described by Mattozzi et al.,[4,5]

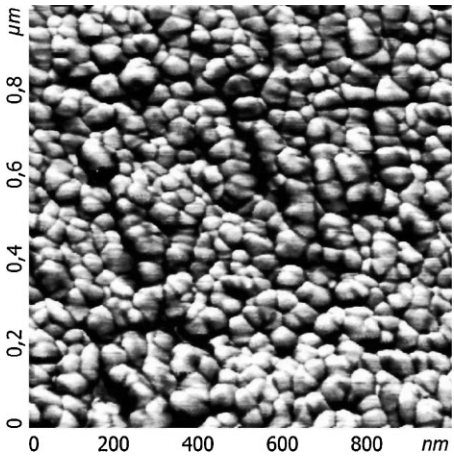

Figure 3.
AFM phase image of sample B (HDPE, $\rho = 0.9394\ g\ cm^{-3}$).

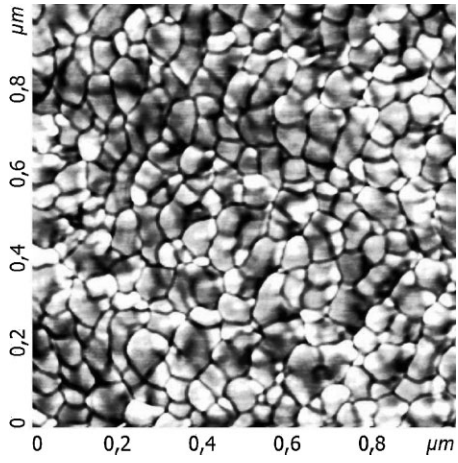

Figure 5.
AFM phase image of sample B (HDPE, $\rho = 0.9394\ g\ cm^{-3}$).

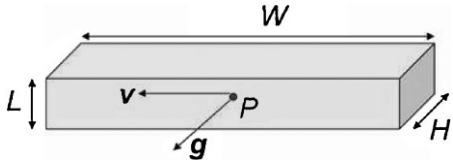

Figure 6.
Basic lamellar element.

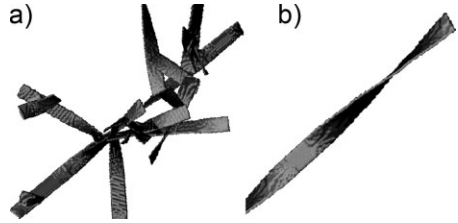

Figure 7.
Lamellar growth (a); (b) twisting.

who were able to reconstruct spherulites with crystallinity up to 30%. Here we present an improved algorithm capable to reconstruct spherulites with a HDPE realistic crystallinities up to 70%. Moreover, our advanced reconstruction algorithm allows to reconstruct spherulites with preferential orientation of lamellae, thus supporting anisotropic penetrant-in-polymer diffusion.

The geometrical simulation of the lamellar growth starts from the single crystal element, which is defined by the position of its center of gravity P, thickness L, width W, height H and by its direction given by vectors v and g, cf. Figure 6.

The growth process is initiated from two opposite sides of the single crystal lamella in directions of vectors g and $-g$. Crystal growth proceeds in subsequent steps by adding further basic crystal elements with the same width, thickness and length as the lamella nucleus. During the growth of the initial lamella the new lamellae are randomly disbranched and start their own growth, cf. Figure 7a. All crystal lamellae also undergo random twisting about their growth direction g, cf. Figure 7b. Probability of both the disbranching and the twisting is controlled by the random number generator. The growth of the crystal lamella proceeds until it collides with other crystal or until the maximum spherulite radius is achieved. Hence, the lengths of lamellae are varied. When the growth of all lamellae is finished, a secondary growth is started to obtain a spherulite structure with roughly spatially uniform distribution of crystalline lamellas that is observed in polyethylene. The algorithm checks the local crystallinity (i.e., volume fraction of crystalline phase) in the resulting spherulite particle and in the regions with insufficient crystallinity starts the growth of new secondary lamellae, which grow from the already existing primary lamellae. This algorithm ensures that the local crystallinity is within acceptable limits, which means approximately $\pm 10\%$ of the average volume crystallinity.

When we want to achieve higher values of crystallinity, we have to apply the stacking of lamellae during primary growth and widening of lamellae after the primary growth. With these improvements we can achieve crystallinites about 70%, which corresponds well to experimental data provided by WAXS measurements. The obtained list of lamellae elements is at the end of the generation discretized to ones (amorphous phase) and zeros (crystalline phase) to the cubic grid and this resulting bitmap (spherulite particle) is visualized in Figure 8.

Diffusion in Reconstructed Semi-Crystalline Polymers

Effective diffusivity of penetrant in semi-crystalline polymer is an important characteristic related to the distribution of amorphous and crystalline phase. Let us introduce the geometrical 3×3 tensor σ into the Fick's law

$$\overline{J} = -D\sigma\overline{\nabla c} \tag{1}$$

where D is the bulk diffusivity, $\overline{J}$ is the space-averaged molar flux intensity and $\overline{\nabla c}$ is the space-averaged concentration gradient. In order to obtain σ, the concentration field in the hetero-phase media, for example, in polymer spherulite, has to be

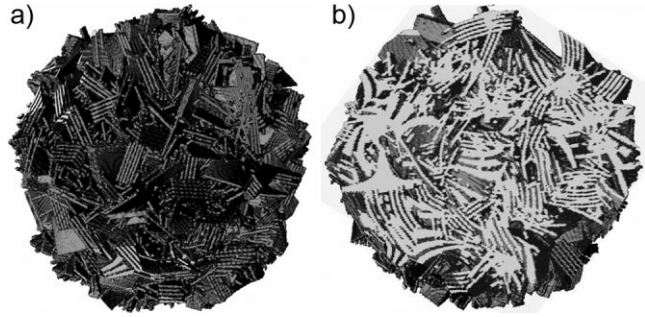

Figure 8.
Digitally reconstructed spherulite particle. (a) whole particle, (b) cut through spherulite.

obtained as the solution of the equation

$$\nabla \cdot (-D\nabla c) = 0, \text{ where}$$
$$D = \begin{cases} 0 & \text{in crystalline phase} \\ 1\times10^{-10}\,\mathrm{m^2/s} & \text{in amorphous phase} \end{cases} \quad (2)$$

Bulk diffusivity in amorphous phase $D = 1 \times 10^{-10}\,\mathrm{m^2/s}$ is set arbitrary because we are interested in the ratio of D^{eff}/D and not in the absolute value of D^{eff}.

The boundary condition of zero flux at the interface between crystalline phase and amorphous phase is imposed. The arbitrary non-zero concentration difference is applied between two opposite walls in the x-direction while zero-flux boundary conditions are applied to remaining four walls. The average molar flux density vector $\overline{J}$ is then evaluated from the computed concentration field $c(x, y, z)$. This allows us to obtain the x-column of the diffusivity geometrical tensor $\boldsymbol{\sigma}$ and the y- and z-columns are consequently calculated in an analogous way. The diffusivity tensor $\boldsymbol{\sigma}$ is symmetrical for isotropic porous medium and the factor is calculated as

$$\psi = D^{eff}/D = tr\sigma/3, \quad (3)$$

where "tr" is the trace operator. The steady state concentration profile in the cubic section of the spherulite particle from which the effective diffusivity is calculated is shown in Figure 9.

The effective diffusion coefficient can be related to the spherulite structure using the tortuosity factor

$$\tau = \frac{\nu_a}{D^{eff}/D}, \quad (4)$$

where ν_a is the volume fraction of amorphous phase ($\nu_a = 1 - \nu_c$). The dependencies of effective diffusivity and tortuosity on crystallinity and lamellae width to thickness (W / L) ratios are shown in Figure 10, respectively. It is evident that the increase in crystallinity causes higher diffusion resistance to transport and the D^{eff}/D ratio decreases. On the other hand tortuosity τ increases.

The spherulite structure with preferred lamellae orientation (Figure 4) were used to study the influence of internal structure on transport properties of semi-crystalline polymers. Table 1 shows the strong influence of crystal orientation on the transport

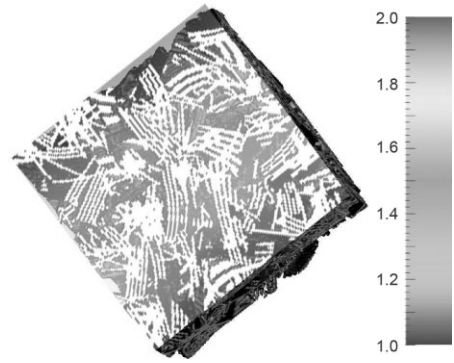

Figure 9.
Steady state concentration profile in reconstructed spherulite particle subjected to dimensionless concentration $c_{\mathrm{left}} = 1$ and $c_{\mathrm{right}} = 2$.

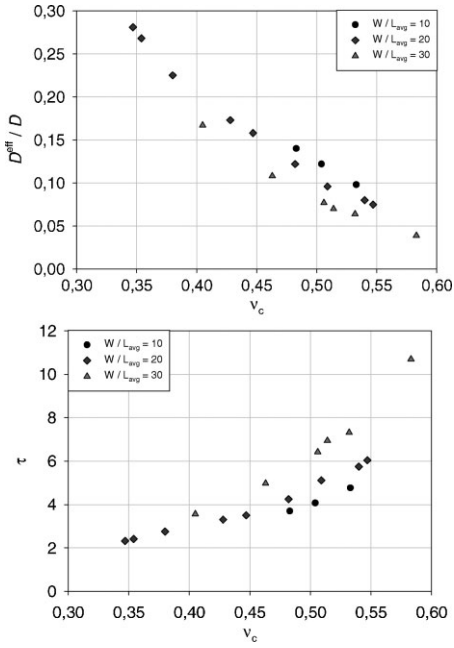

Figure 10.
Dependency of effective diffusivity and turtuosity on crystallinity ν_c and width-to-thickness ratio W/L of lamellae.

Table 1.
Anisotropic diffusion.

Direction	X	Y	Z
D^{eff}/D	0.164	0.274	0.159

properties. Coefficient in this table correspond to spherulite with volume crystallinity $\nu_C = 0.50$.

Conclusion

The general methodology of linking the semi-crystalline structure of polyolefins to their application properties has been proposed and illustrated on the example of penetrant diffusion. The methodology consists of following steps: (i) AFM imaging of crystalline structure including a proper method of sample preparation, (ii) processing of AFM images and their systematic description by morphology descriptors, (iii) reconstruction of spatially 3D replica of semi-crystalline polymer having the same morphology descriptors as the imaged sample, (iv) calculation of application properties depending on spatially 3D distribution of crystalline and amorphous domains, (v) validation of the whole methodology by comparison with independent experimental data, e.g., with data on penetrant diffusion in polymer.

The work on the proposed methodology hasn't been finished yet, especially in the part of statistical characterization of semi-crystalline structure by suitable morphology descriptors. AFM images obtained so far can't be automatically binarized by either threshold-based, gradient-based or nonlocal-thersholding-based algorithms. Nevertheless, we demonstrated mapping of sub-micron sized spherulites by AFM as well as primary crystalline domains in etched samples. Dry etching by oxygen plasma enabled obtaining of better-quality AFM images displaying short-distance ordering of crystalline domains than wet etching. We are able to analyze samples with preferentially oriented crystallites and we found that the morphology of some HDPE samples resembles granular-like morphology.

The subject of our studies are nascent polyolefin particles collected at reactor outlet or standard testing specimens of polyolefin samples. Therefore, we are analyzing samples with no special treatment affecting their crystallization.

One of major achievements of this work is the geometrical reconstruction of spherulites by the lateral growth of lamellae from nucleation center, by their braching, twisting and stacking yielding crystallinity of reconstructed spherulites up to 70%. Modeling of penetrant diffusion in semi-crystalline polymer and evaluation of effective diffusivity from simulated data has been also mastered.

Acknowledgements: Support from projects GA CR 106/10/1912 and KAN208240651 is acknowledged.

[1] C. Slusarczyk, Time resolved SAXS investigations of morphological changes in a blend of linear and branched polyethylenes during crystallization and subsequent melting, *Journal of Alloys and Compounds*, **2004**, *68*, 382.
[2] H. Zhou, G. L. Wilkes, Comparison of lamellar thickness and its distribution determined from DSC, SAXS, TEM and AFM for high-density polyethylene films having a stacked lamellar morphology, *Polymer*, **1997**, *38*, 5735.
[3] D. C. Bassett, *Principles of polymer morphology*, Cambridge University Press, 1. edition. **1981**.
[4] A. Mattozzi, P. Serralunga, M. S. Hedenqvist, U. W. Gedde, Mesoscale modelling of penetrant diffusion in computer generated polyethylene spherulite-like structures. *Polymer* **2006**, *47*, 5588–5595.
[5] A. Mattozzi, M. Minelli, M. S. Hedenqvist, U. W. Gedde, Computer-built polyethylene spherulites for mesoscopic Monte Carlo simulation of penetrant diffusion: Influence of crystal widening and thickening. *Polymer* **2007**, *48*, 2453–2459.
[6] S. Bensason, J. Minick, A. Moet, S. Chum, A. Hiltner, E. Baer, Classification of homogeneous Ethylene-Octene copolymers based on comonomer content, *Journal of Polymer Science*, **1996**, *96*, 1301–1315.
[7] H. Y. Chen, S. P. Chum, A. Hiltner, E. Baer, Comparison of Semicrystalline Ethylene - Styrene and Ethylene – Octene Copolymers based on Comonomer Content, *Journal of Polymer Science*, **2001**, *9*, 1578–1593.
[8] R. H. Olley, D. C. Bassett, An improved permanganic etchant for polyolefines, *Polymer*, **1982**, 1707–1710 UK.

